AD-A214 771

# REPORT DOCUMENTATION PAGE

Form Approved
OMB No. 0704-0188



| 1. AGENCY USE ONLY (Leave blank) | 2. REPORT DATE | 3. REPORT TYPE AND DATES COVERED |
|---|---|---|
| | April 1984 | Final (15 Sep 83/14 Mar 84 |

4. TITLE AND SUBTITLE

LIQUID FILM FOR SPACECRAFT SURVIVABILITY TO LASER RADIATION

5. FUNDING NUMBERS

FQ8671-8301502

3005/A1

AUTHOR(S)

M. Frish, A. Gelb, H. Legner, L. Cowles

7. PERFORMING ORGANIZATION NAME(S) AND ADDRESS(ES)

Physical Sciences Inc
Research Park, P.O. Box 3100
Andover, MA 01810

8. PERFORMING ORGANIZATION REPORT NUMBER

1658

AFOSR-TR-89-[illegible]

9. SPONSORING/MONITORING AGENCY NAME(S) AND ADDRESS(ES)

AFOSR
BLDG 410
BAFB DC 20332-6448

10. SPONSORING/MONITORING AGENCY REPORT NUMBER

F49620-83-C-0155

11. SUPPLEMENTARY NOTES

DTIC
ELECTE
NOV 30 1989
S B D

12a. DISTRIBUTION/AVAILABILITY STATEMENT

12b. DISTRIBUTION CODE

13. ABSTRACT (Maximum 200 words)

The thin liquid film mediated laser interaction concept has been ivestigated in a joint-experimental theoretical effort.

The experimental portion of the program has demonstrated the laser hardening capability of thin liquid films for graphitic substrates. Measurements of film stability and optical reflectivity of coated graphite samples were made under simulated c.w. laser heating in an electron beam apparatus. The results were that the films remained intact at temperatures of 3300 K and for high rates of substrate vaporization. Measured surface emissivities were maintained at low values throughout the heating period. Values of Q*, the laser energy per gram of carbon vaporized, were increased by factors of 3-4 over that for graphite and 2-3 over that for TBR materials. Heats of vaporization were measured and found similar to uncoated graphite.

| 14. SUBJECT TERMS | 15. NUMBER OF PAGES |
|---|---|
| | 53 |
| | 16. PRICE CODE |

| 17. SECURITY CLASSIFICATION OF REPORT | 18. SECURITY CLASSIFICATION OF THIS PAGE | 19. SECURITY CLASSIFICATION OF ABSTRACT | 20. LIMITATION OF ABSTRACT |
|---|---|---|---|
| unclassified | unclassified | | |

NSN 7540-01-280-5500

Standard Form 298 (890104 Draft)
Prescribed by ANSI Std 239-18
298-01

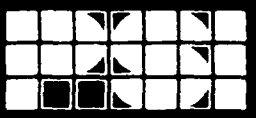

PSI TR-419



# PHASE I. THE USE OF LIQUID FILM FOR SPACECRAFT SURVIVABILITY TO LASER RADIATION

FINAL REPORT

for the period

15 September 1983 - 14 March 1984

M. Frish, A. Gelb, H. Legner and L. Cowles

April 1984

Prepared for

Air Force Office of Scientific Research
Bolling AFB, DC 20332

**PHYSICAL SCIENCES INC.**
RESEARCH PARK, ANDOVER, MA 01810

PROJECT SUMMARY

The thin liquid film mediated laser interaction concept has been investigated in a joint-experimental theoretical effort.

The experimental portion of the program has demonstrated the laser hardening capability of thin liquid films for graphitic substrates. Measurements of film stability and optical reflectivity of coated graphite samples were made under simulated c.w. laser heating in an electron beam apparatus. The results were that the films remained intact at temperatures of 3300 K and for high rates of substrate vaporization. Measured surface emissivities were maintained at low values throughout the heating period. Values of Q*, the laser energy per gram of carbon vaporized, were increased by factors of 3-4 over that for graphite and 2-3 over that for TBR materials. Heats of vaporization were measured and found similar to uncoated graphite.

The theoretical portion of the program identified film stability criteria and mechanisms of mass transport through the coating material. Maps were constructed for ranges of film stability as a function of film thickness and thermal gradients. Thermochemical calculations were made to predict equilibrium vapor pressures above the coated samples.

The results of this program establish the feasibility of the thin liquid film mediated laser interaction concept.

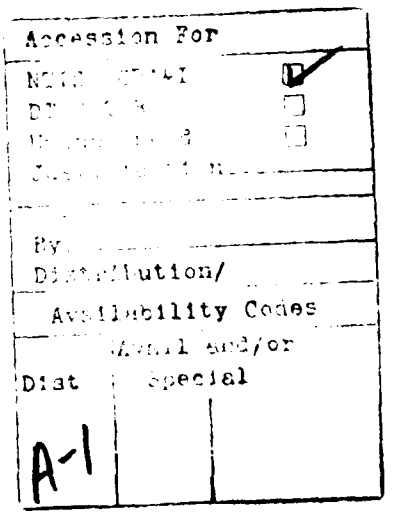

ACKNOWLEDGEMENTS

The authors would like to acknowledge the most useful and inciteful advice of the internal PSI reviewer for this program, Dr. Gerald Wilemski. Additionally, we would like to acknowledge Mr. R. Cole of JetCom Inc. for his skill in the art of sample preparation and Dr. P. N. Nebolsine of PSI for technical direction.

TABLE OF CONTENTS

FIGURES

# 1. INTRODUCTION

The survivability of US satellites to high power laser radiation has become a key issue since the advancement of high power lasers as weapons has been extended to strategic scenarios. Thus far, the US Air Force has directed most of its efforts toward the protection of essential thermal control, communication and optical systems against ground based CW lasers. Passive laser resistant materials concepts have been developed as part of the SMATH (Satellite Materials Hardening) program (initiated by the Air Force Materials Laboratory) for use against ground based IR lasers. These materials concepts were designed to be both highly reflective and emissive against tens of watts/cm$^2$ of laser flux through the use of thin dielectric and metallic material layers.

For laser intensities significantly greater than those contemplated for near term CW laser systems, a new generation of innovative concepts must be proposed and developed to insure spacecraft survivability. Present approaches are not adequate at laser fluxes which will vaporize or melt thin layers. It is necessary to devise materials concepts which are highly laser resistant because of their ability to absorb and dissipate the incoming energy or utilize techniques which will block the absorption of laser radiation.

Approaches to protecting spacecraft from high intensity laser radiation include: (1) covering the spacecraft with a material which is highly resistant to laser irradiation, and (2) dispersion of absorbing (or reflecting or scattering) media in space in between the laser beam and the spacecraft. The first approach involves managing the incident laser flux so that it deposits as little heat and removes as little mass as possible; the second approach blocks the beam from reaching the spacecraft.

In the Phase I program PSI investigated the concept of thin liquid film mediated laser interaction, a hardening scheme which is an example of approach (1). The concept consists of coating a material to be laser hardened with a thin film of another material which liquefies at temperatures well below the substrate vaporization temperature. Hence, upon laser irradiation, a thin liquid film coats the substrate. The liquid film has a dual role:

(1) it is reflective to laser radiation and (2) it is maintained on the surface while allowing substrate vapor to escape. Laser hardening is provided by the reflectivity of the liquid film. Stable films are possible with films that act as permeable membranes to substrate vapor. The critical issues for a the feasibility of the thin liquid film mediated laser interaction concept are the development of coating materials that are highly reflecting liquids, can transport substrate materials, and are not removed from the substrate (i.e., form stable films) during a laser encounter.

The Phase I program was a combined experimental-theoretical effort designed to establish the feasibility of the thin film mediated laser interaction concept. The goals of the experimental effort were to test tungsten carbide coated graphite under simulated CW laser irradiation. The theoretical portion of the program examined models for carbon vapor transport through the tungsten carbide and the equilibrium thermodynamics of tungsten-carbon systems. The most significant results are summarized below.

Samples of ATJS graphite coated by plasma spraying with 125 μm of tungsten carbide (WC) (88% WC, 12% Co) were prepared. These samples were heated under simulated CW laser conditions to ~ 3300 K. The peak temperatures were maintained for sufficient periods of time so that a substantial amount of the graphite substrate was vaporized. The emissivity and heat of vaporization were determined. The following observations were made: (1) the coating withstood the heating and carbon vaporization, (2) the measured surface emissivity was determined to be ~ 0.25, a value characteristic of the tungsten carbide coating not of the graphite substrate (emissivity ~ 0.8), (3) the heat of vaporization was determined to be ~ 30 kJ/g indicating ordinary carbon vaporization, and (4) post-heating Auger analysis of vaporization products showed no evidence of tungsten removal from the surface.

Fluid mechanical calculations indicated that, under the high heating conditions in our experiments, induced convection can occur and possibly provide sufficiently rapid transport of carbon vapor through the film to prevent film removal. A potential bubbling mechanism for transport has also been identified. Thermochemical calculations show that at 3300 K and with an initial surface composition of WC, ordinary carbon vaporization ($C_3$ the dominant

vapor species) should occur and should persist if carbon transport through the liquid film is rapid.

The significance of these results for laser hardening is that we have demonstrated that a thin, liquid, tungsten carbide coating on graphite increases the value of $Q^*$, the laser energy required per unit mass removed, by a factor of approximately 3-4. This value of $Q^*$ is even superior, by a factor of 2-3, to that of a TBR (tungsten bearing resin) type material. Moreover, the coating is stable under high heating, has a minimal associated weight penalty and may also be useful for nuclear hardening. These results establish the feasibility of the concept of thin liquid film mediated laser interaction for laser hardening and mandate further investigation leading towards development of the concept.

## 2. EXPERIMENTAL STUDIES

### 2.1 Introduction

The goal of the Phase I experiments were to demonstrate that, under proper conditions, a thin coating of tungsten or tungsten carbide applied to a carbonaceous substrate would maintain its integrity and offer superior resistance to laser irradiation. Laser hardness is enhanced both by increasing the reflectivity of the irradiated surface or by increasing the heat of ablation of an ablating surface. A refractory metal carbide coating on a carbon surface offered the potential to improve hardness through both of these mechanisms. Experiments to date have confirmed that coatings of tungsten carbide applied to ATJS graphite in thickness exceeding 75 μm, in fact, give excellent reflectivity but do little to enhance the heat of ablation. It is notable that these coatings remained intact and highly reflective while the materials were heated by an electron beam to temperatures in excess of 3300 K, and a considerable volume of carbon was vaporized from below the coating. The following subsections explain and document these results in detail.

### 2.2 Sample Preparation

Tungsten carbide was deposited on flat ATJS graphite surfaces by plasma spraying. The deposition was performed by JETCOM Inc. of Wilmington, MA, as was the sample surface preparation which was required for good bonding. The powder sprayed onto the surface included up to ten weight percent of cobalt to enhance sticking. Square samples, 2.54 cm per side, were manufactured with nominally 25, 75 or 125 μm thick coatings, and these samples were subsequently machined into disks of 1 cm diameter and 1 mm thickness for study in the PSI electron-beam high temperature materials evaluation laboratory. A brief description of this apparatus follows.

## 2.3 Description of e-beam laboratory[1]

The PSI materials evaluation laboratory employs a low energy (< 10 kV), moderate power (< 2.5 kW) electron beam to heat target materials to temperatures at which approximately 15% of the supplied power is consumed by vaporization of the target. For 1 cm diameter, 1 mm thick carbon disks, the target temperature which is achieved under these conditions is approximately 3300 K. Front surface temperatures of the targets are measured with better than ± 3.5% accuracy by a three-color pyrometer and capabilities exist to measure spectral emissivities at 2.7, 3.8, and 10.6 μm, total emissivities, specific heats, and heats of vaporization for virtually any refractory material.

Previous work with this apparatus has revealed dramatic changes in the spectral emissivity of a variety of carbonaceous materials upon massive vaporization of their surfaces. For example, the 10.6 μm emissivity of uncoated ATJS is shown in Fig. 2.1 to increase dramatically from about 0.6 in its pre-vaporized state to nearly 1.0 with the removal of about 20% of the target's initial mass. In contrast, Fig. 2.2 shows the behavior of a metal loaded carbon/carbon matrix such as TBR.* Here, the emissivity decreases upon vaporization due to the formation of a metallic layer on the target surface. However, both of these materials were found to have similar heats of vaporization, about 30 kJ/g, which is roughly the value which results from vaporization of an equilibrium mixture of carbon vapor species.

For the present work, spectral emissivities at 10.6 μm or 3.8 μm of the coated graphite targets were measured along with their heats of vaporization. In addition, glass slides to collect condensible vapors were placed approximately 25 cm in front of the target, thereby allowing elemental determination of the material which was removed from the target. Partially vaporized targets were saved for post-mortem analysis.

*These measurements were performed as part of the Laser Countermeasures Materials Development Program sponsored by the Defense Advanced Research Projects Agency (Contract No. S322-0L7200).

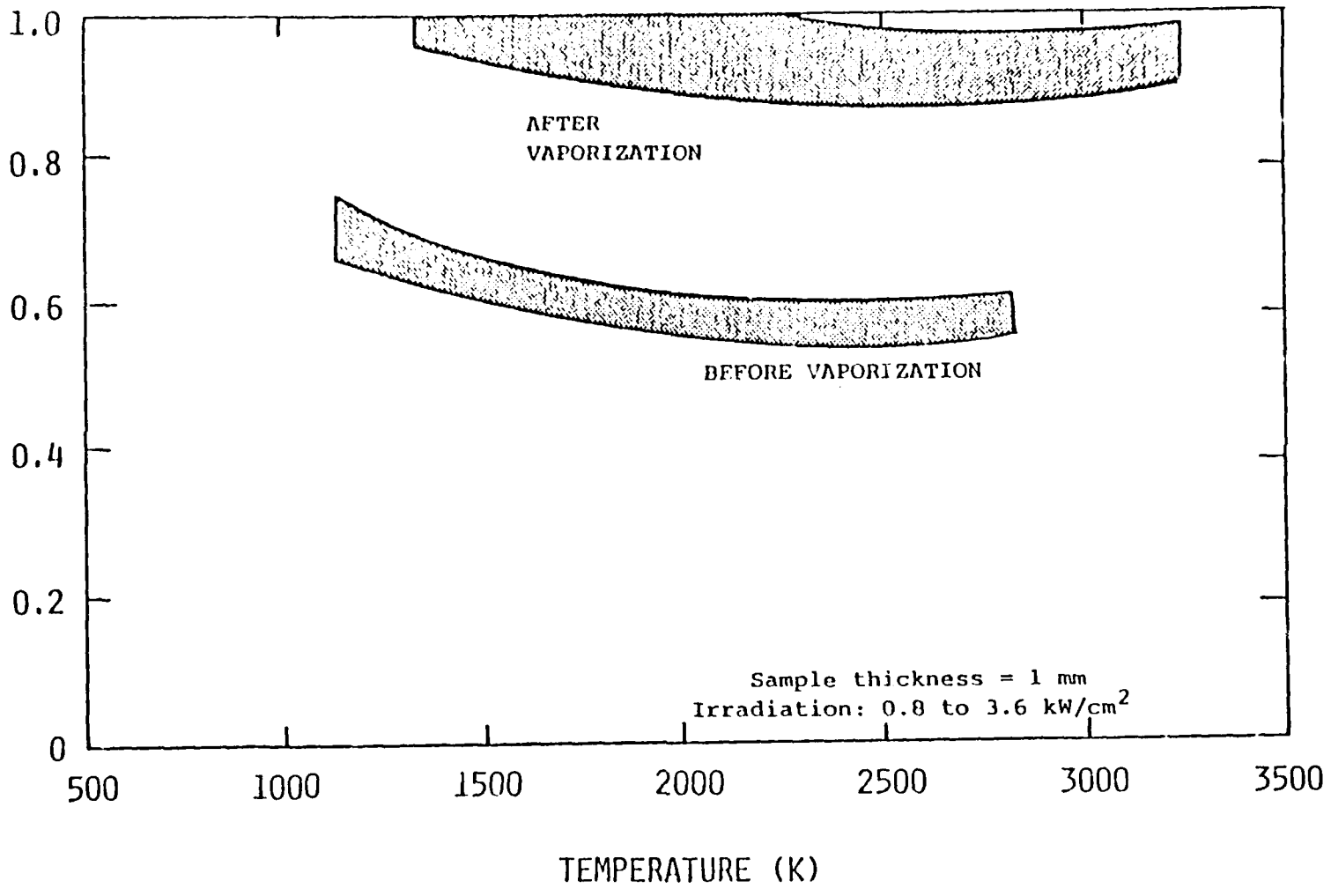


Fig. 2.1 ATJS - 10.6 μm emissivity vs. temperature.

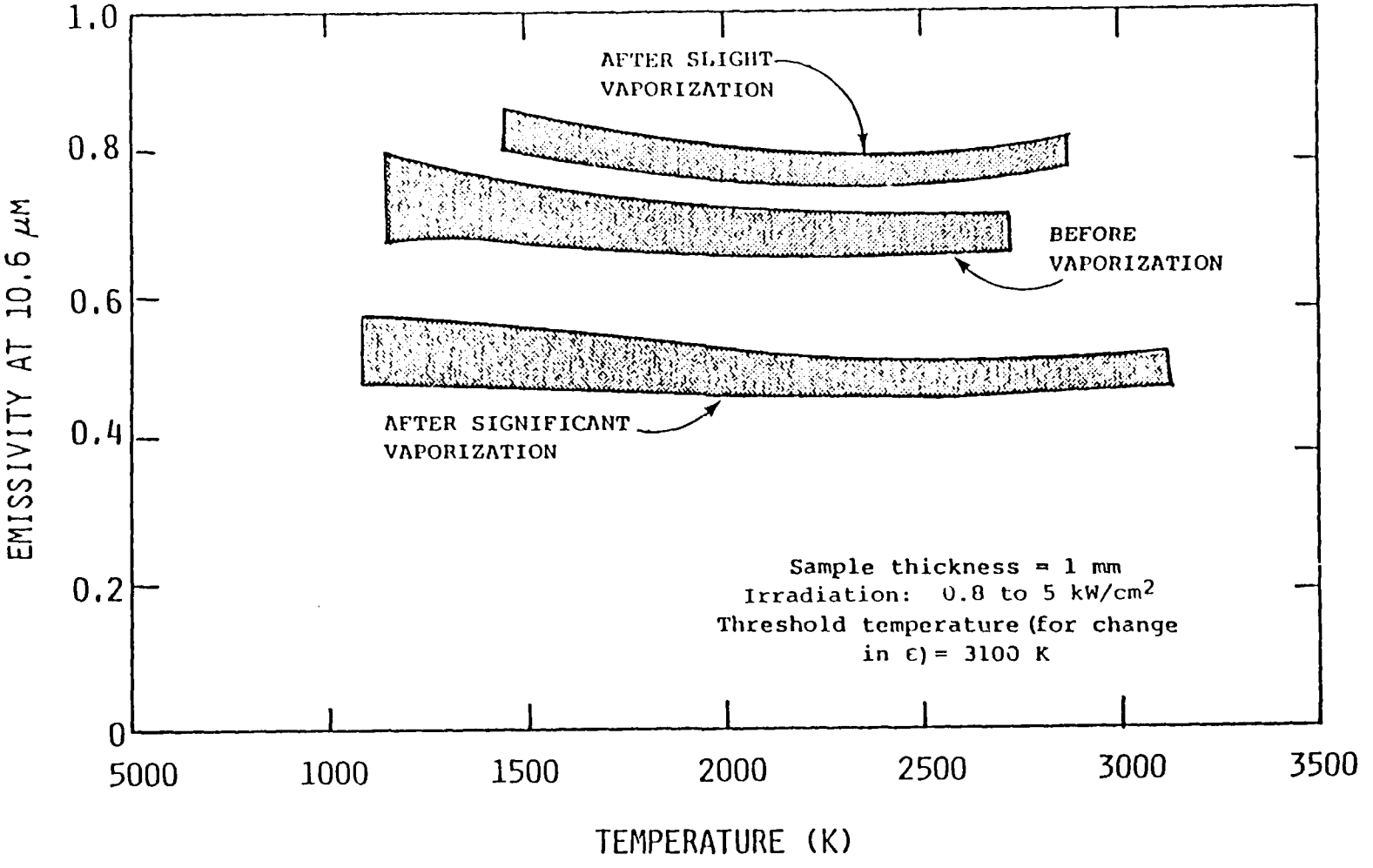


Fig. 2.2 10.6 μm emissivity vs. temperature of a TBR class material.

## 2.4 Experimental Results

Figure 2.3a shows the temperature and spectral emissivity at 10.6 μm histories during the vaporization of a target with a 125 μm coating. At time t = 0 the electron beam is switched onto the target with about 1.2 kW of power. The power density is about 5 $kW/cm^2$. Since there is no reflection of electrons, but the reflectivity of the surface at a threat laser wavelength is measured to be about 75%, this corresponds to a laser intensity of roughly 20 $kW/cm^2$. The temperature rapidly increases to its steady state value of 3340 K and holds these for 1 second, at which time the power is switched off and the target cools. During this time, 20 mg of the initially 100 mg target were removed, with a heat of vaporization measured to be 32.5 ± 12 kJ/g. The 10.6 μm emissivity throughout this period is seen to change only slightly and maintains a value below 0.3 throughout. Similar experiments in which sufficient material was removed to pierce the target showed no change in this behavior. Figure 2.3b shows similar histories, but with a target irradiated with 700 W (~3.5 $kW/cm^2$) of e-beam power, and the spectral emissivity measured at 3.8 μm. In this case, the temperature rises relatively slowly, and exhibits a temporary constancy while the coating melts. The 3.8 μm emissivity decreases from an initial value of ~ 0.4 before the melt, to a final value of about 0.25 afterwards. The lower value again maintains upon cooling.

For comparison, Fig. 2.4 shows the temperature and emissivity histories for a pure WC target, and similarly for a TBR class of material in Fig. 2.5. The tungsten carbide undergoes a melting transition during heating, at which time the initially rough surface takes on a smooth, highly reflective apppearance, as indicated by the drop in emissivity at that time. Upon cooling, the shininess is maintained and the emissivity remains low even after resolidification. The spectral emissivity value of 0.23 (at 3.8 μm) is the lowest value that can be expected for a tungsten carbide coating and is nearly equal to that achieved with the coated graphite. In contrast, the emissivity at 2.7 μm of the TBR material has an initial value of 0.6, increases briefly to 0.9, and finally decreases to a final value of about 0.6 at high temperature. Since low emissivities (or equivalently, low absorptivities, $\alpha$, and high reflectivities, R, where $R = 1 - \alpha$) are desirable for laser hardness, the WC coated graphite appears to have superior properties.

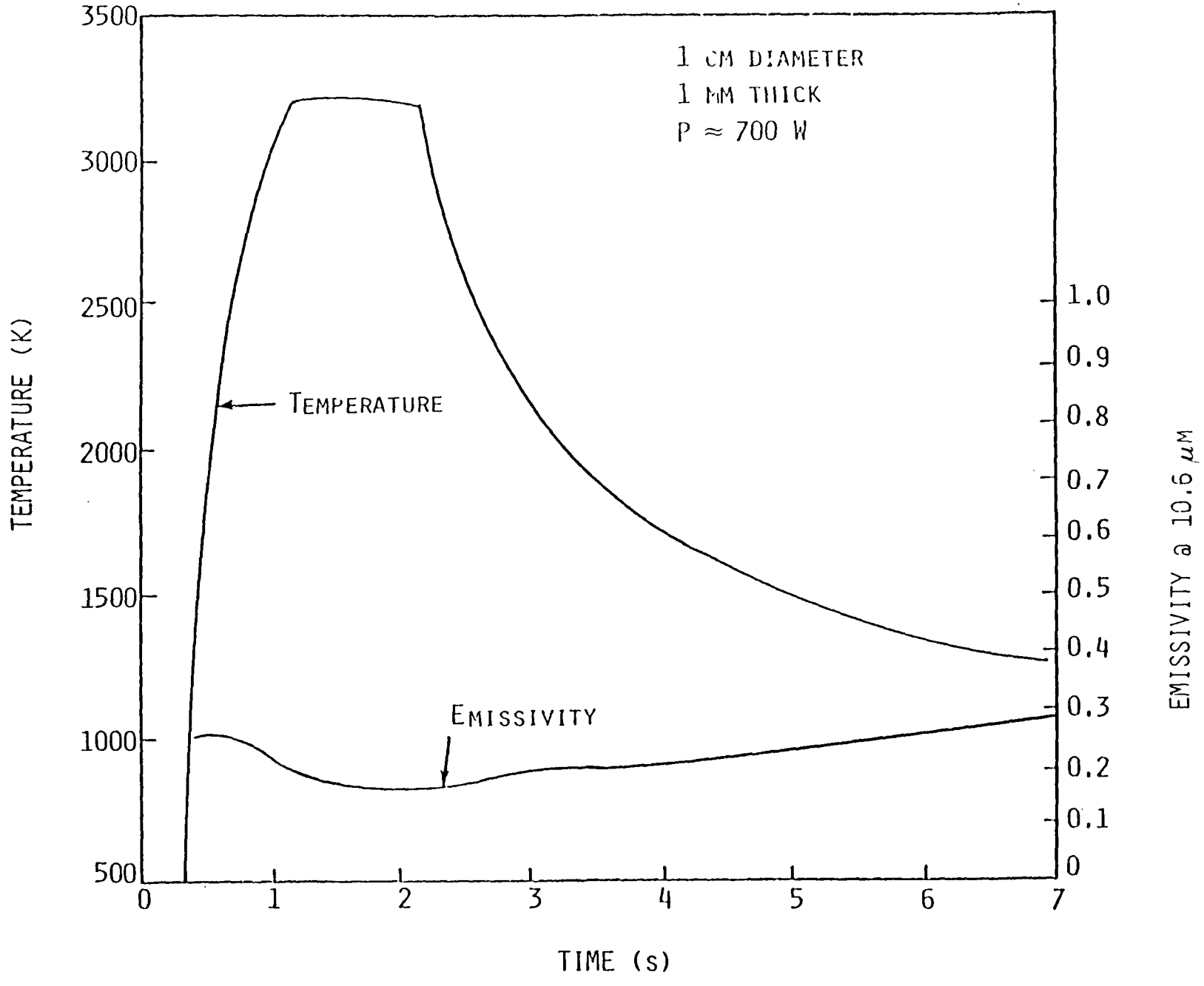


Fig. 2.3a Temperature and emissivity vs. time for target #3.

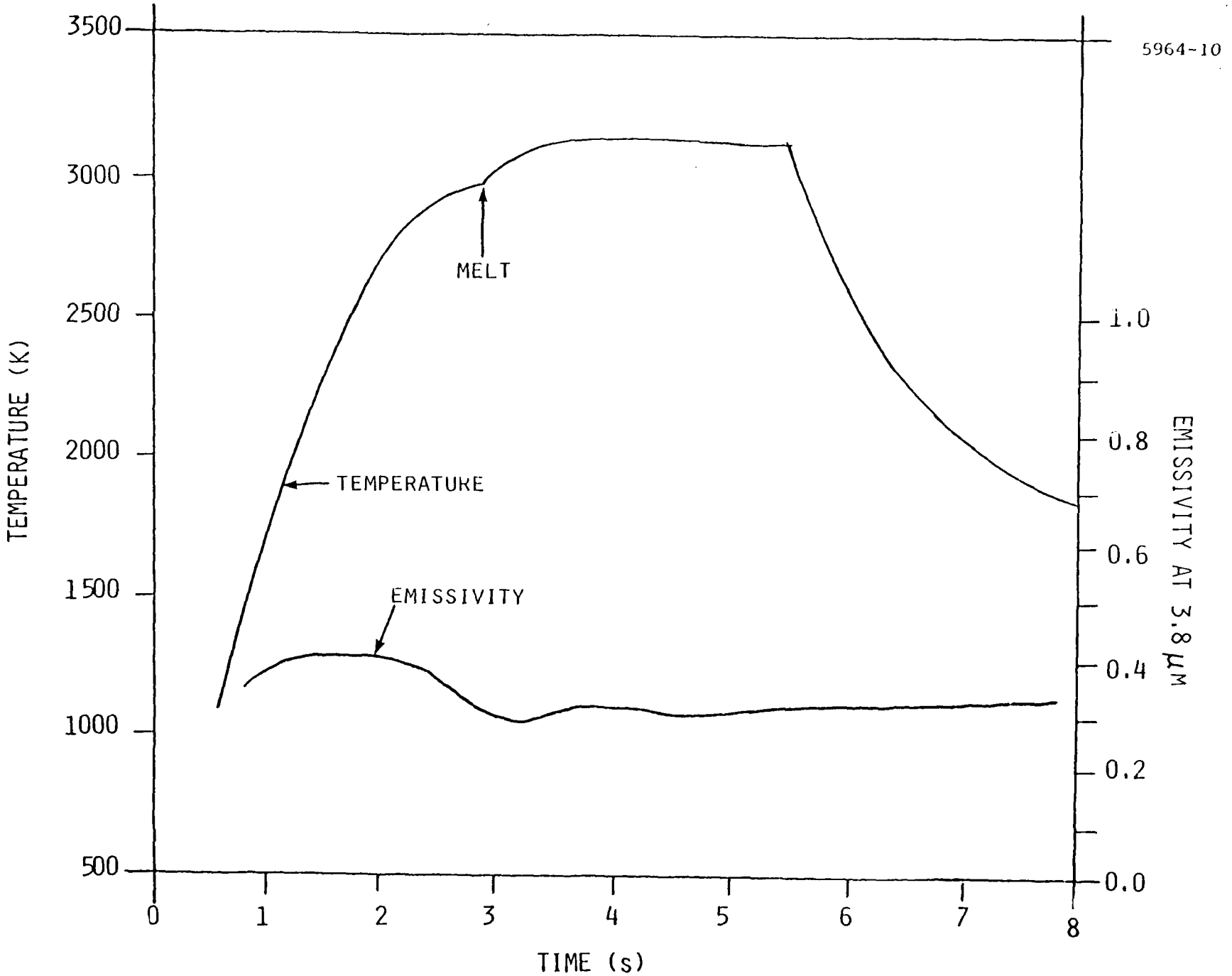


Fig. 2.3b Temperature histories of 125 μm thick WC coating on ATJ-S graphite at low flux and spectral emissivity at 3.8 μm.

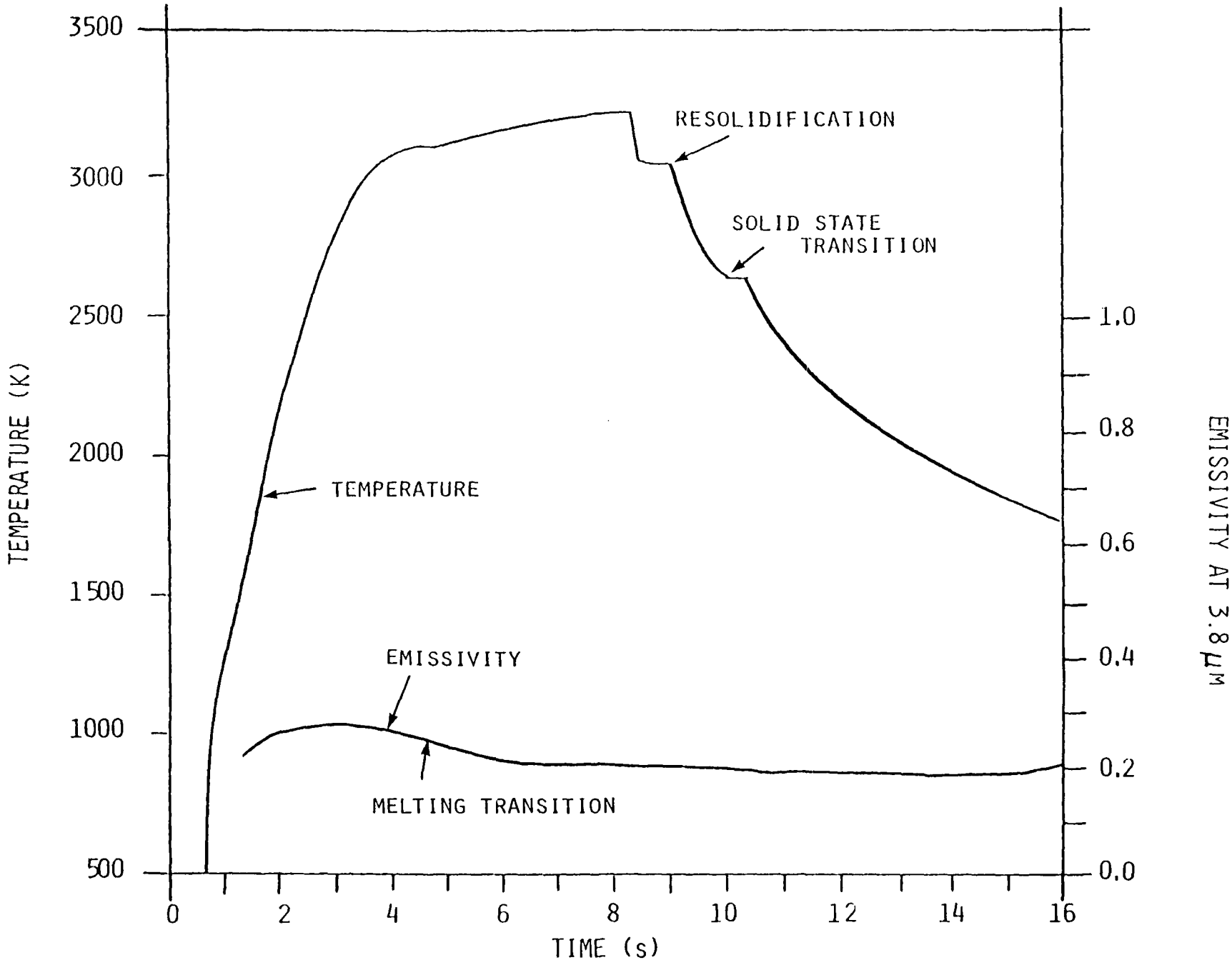


Fig. 2.4 Temperature and spectral emissivity histories of WC target.

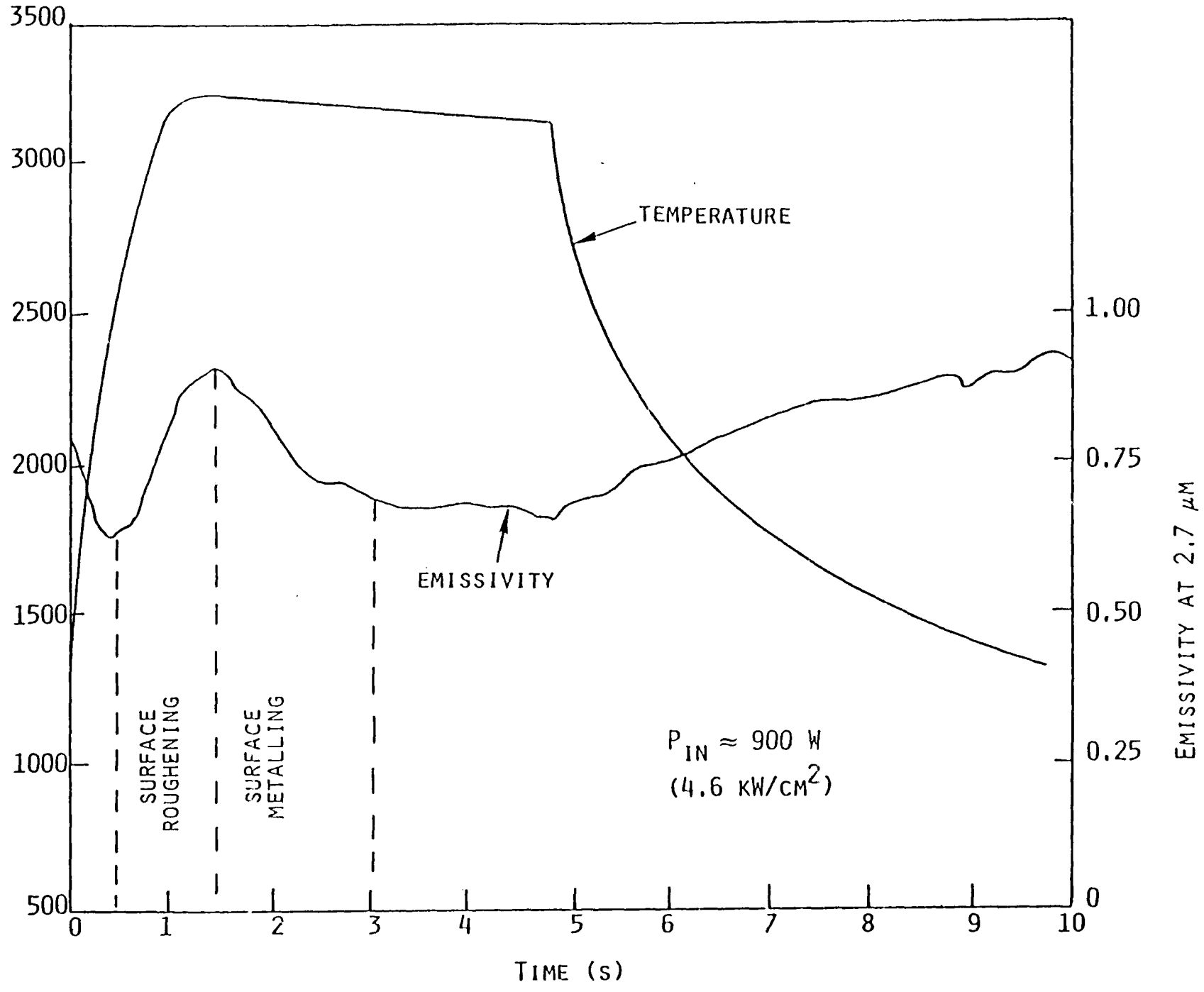


Fig. 2.5 Emissivity at 2.7 μm and temperature histories of a TBR-like target.

Samples with 75 μm thick coating behaved similar to those with 125 μm coatings. However, the 25 μm thick showed a dramatic change when the target began rapid vaporization. Figure 2.6 shows the temperature and emissivity histories for such a target. Although the emissivity starts off with a value of about 0.3, upon reaching a temperature of 3000 K, the emissivity rapidly increases to 0.6.

Post-vaporization examination of these targets indicates immediately the reason for the continuously high reflectivity of the thicker coated samples, and the loss of reflectivity of the 25 μm coating. Although a substantial amount of graphite was removed from the front surface of each target, as indicated by craters in the surfaces, the thicker carbide layers remained as coatings on the craters, while the 25 μm coating was removed thereby exposing the graphite substrate. Optical photomicrographs of three representative targets are presented in Figs. 2.7a-c. Auger analysis of the material collected on the glass condensation plates during irradiation of a 125 μm coated target indicates only carbon and cobalt, no tungsten, thus proving that the crater resulted from vaporization of the substrate only. Figures 2.8a & b show scanning-electron-microphotographs (SEM) of the cross-section of this cratered-surface; the bright layer is the coating. Figures 2.9a & b are SEMs of the front surface of the target in regions (a) where vaporization has occurred, and (b) outside of the vaporization zone. Comparison of these two photos shows that, although the tungsten carbide coating remained intact, its morphology appears to have been altered by the vaporization. In the vaporized zone, the coating has the appearance of interconnected dish-shaped globules. Elsewhere, the coating is comprised of a continuous layer of connected, irregularly shaped particles with occasional voids. These data suggest that, in the vaporized region the tungsten carbide coating melted while the substrate graphite vaporized and pitted the surface. The coating filled in the pits and, upon cooling and resolidification, formed the observed globular structures, cross sections of which are shown at two magnifications in Figs. 2.10a & b. Their smoothness, and the sphericity of their bottom surfaces are further indications that they resolidified from a melt in which surface tension was a dominant force in determining their shape.

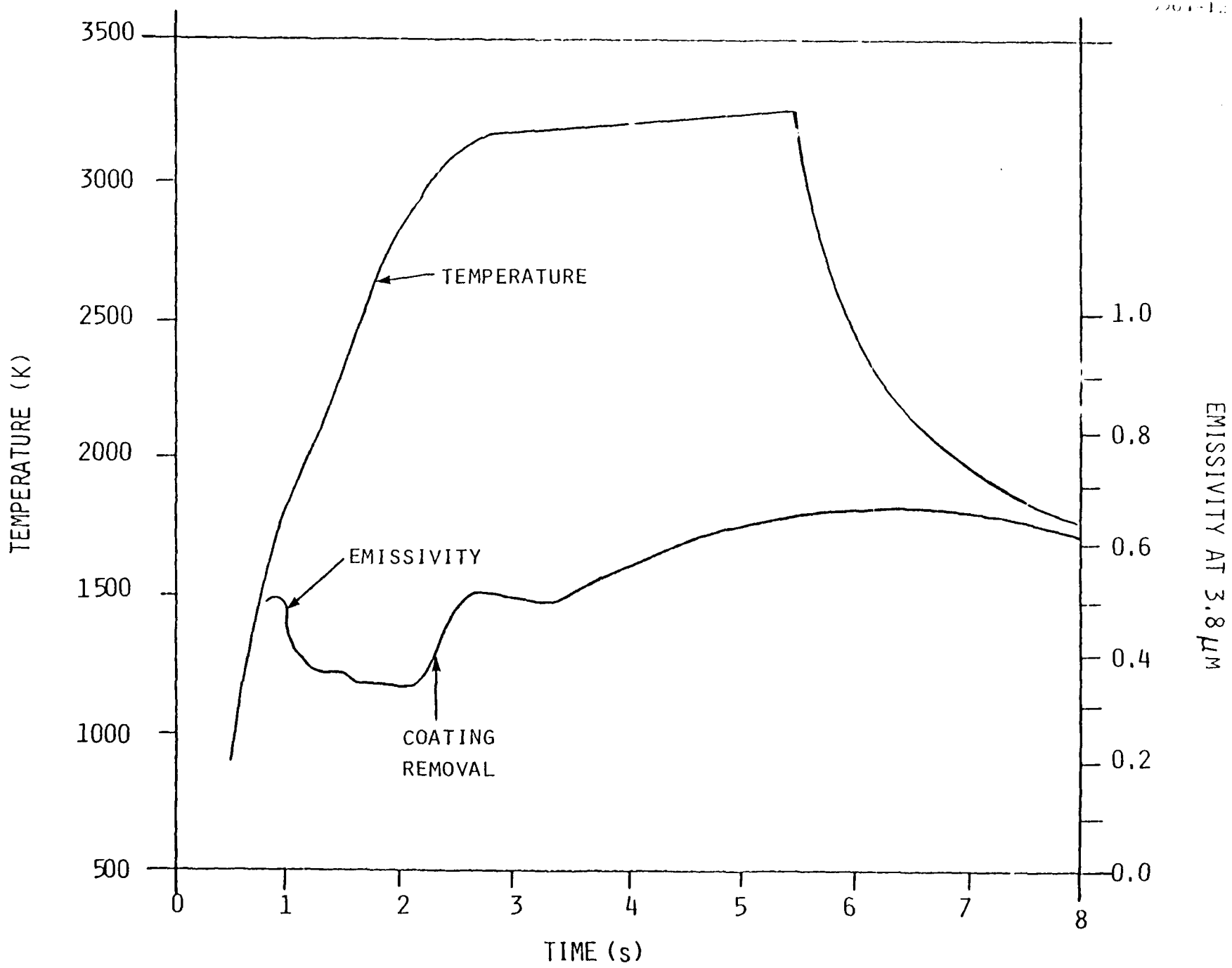


Fig. 2.6 Temperature and spectral emissivity histories of 25 μm coated target.

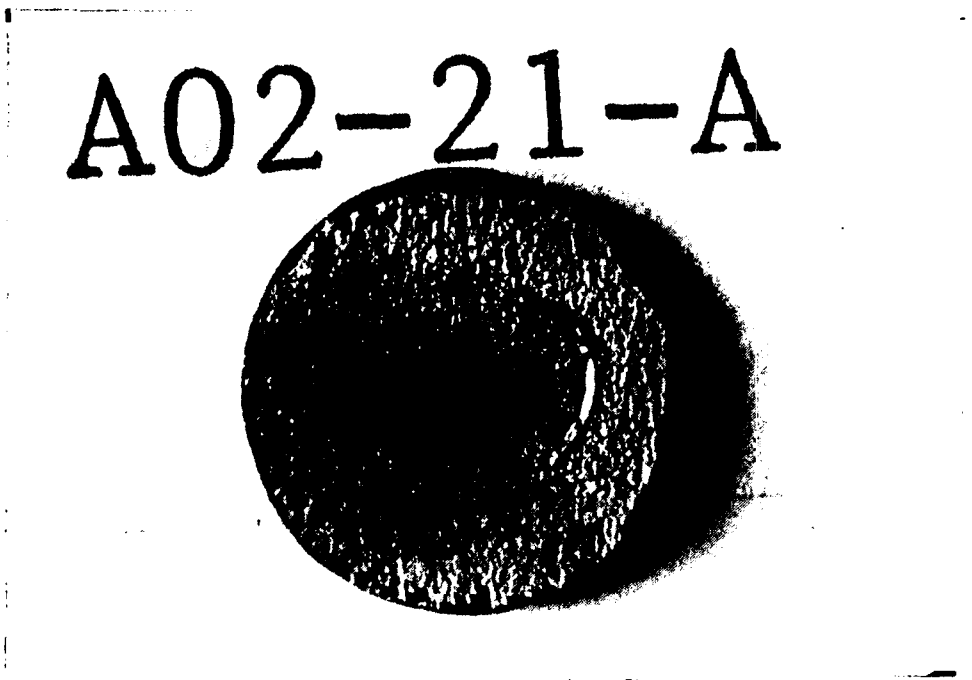


Fig. 2.7a ATJS target coated with 25 μm WC.
Note exposure of graphite at center of irradiated target.

5995-1b

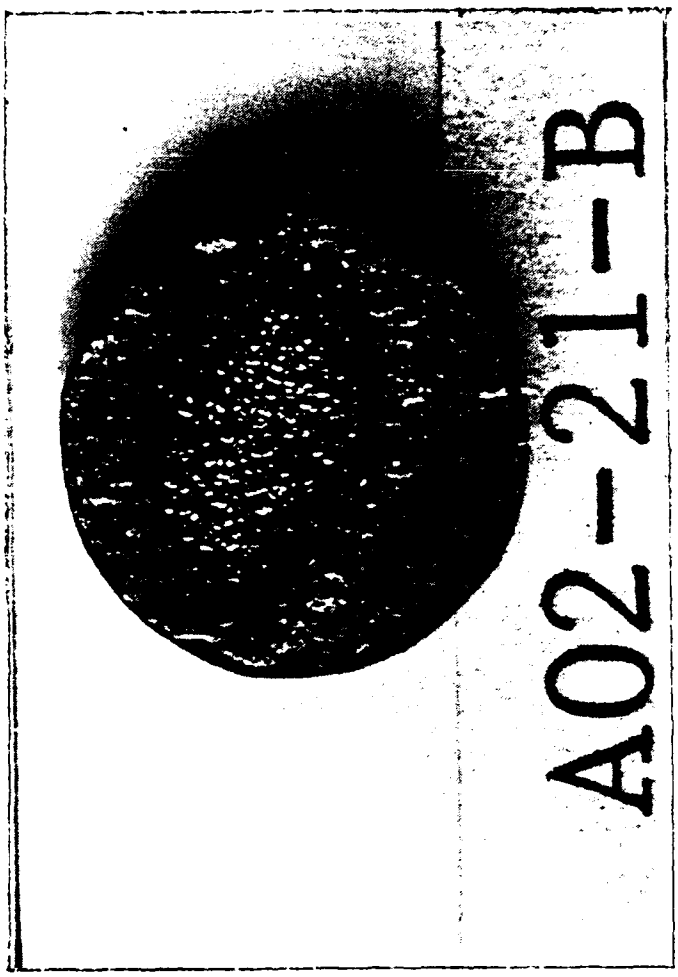


Fig. 2.7b ATJS target coated with 75 μm WC.

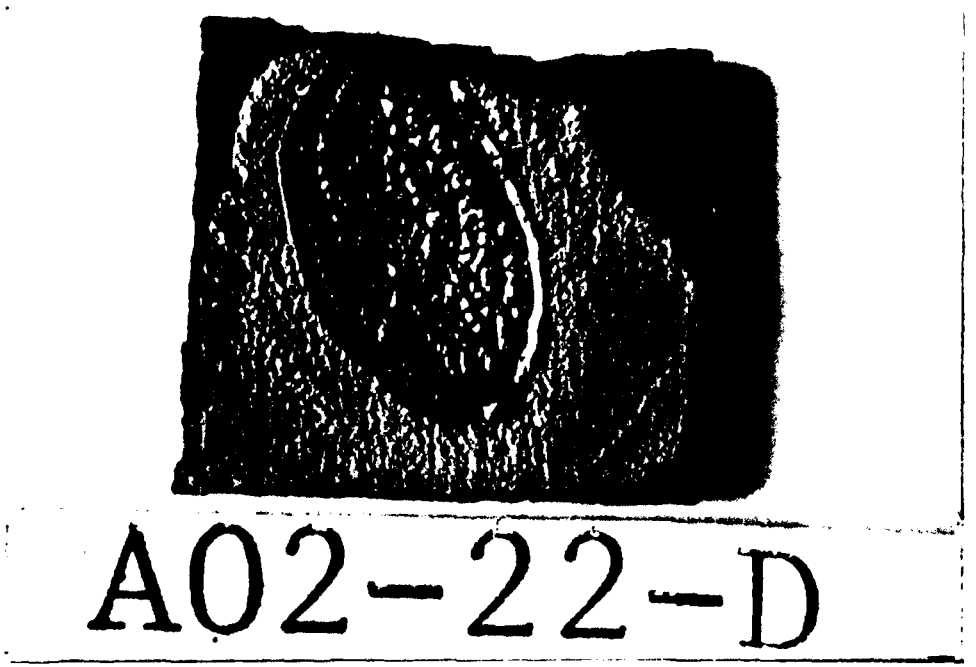


Fig. 2.7c ATBS target coated with 1.25 μm WC.

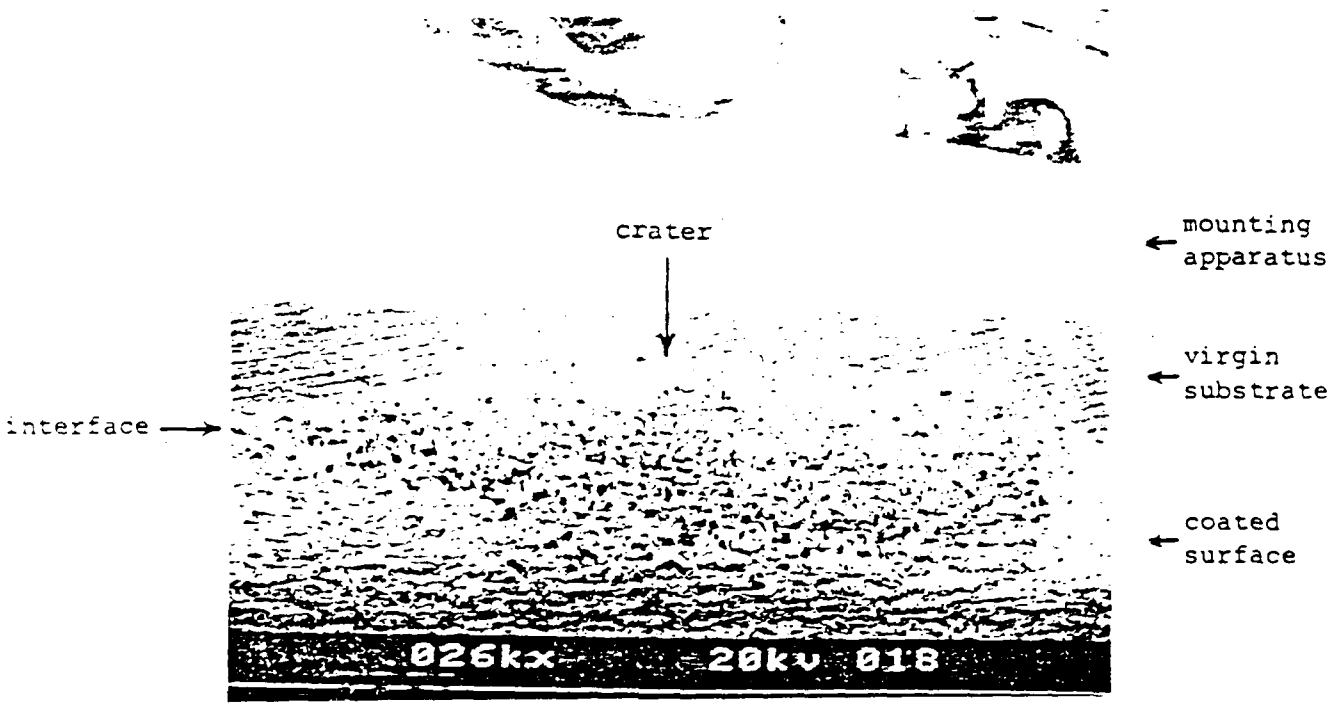


Fig. 1.8a Electron photomicrograph at 26x of cross section of partially vaporized target. This sample was observed at a 30° angle with a large depth of field. Lack of depth perception makes the thin coated surface appear to fill in the crater.

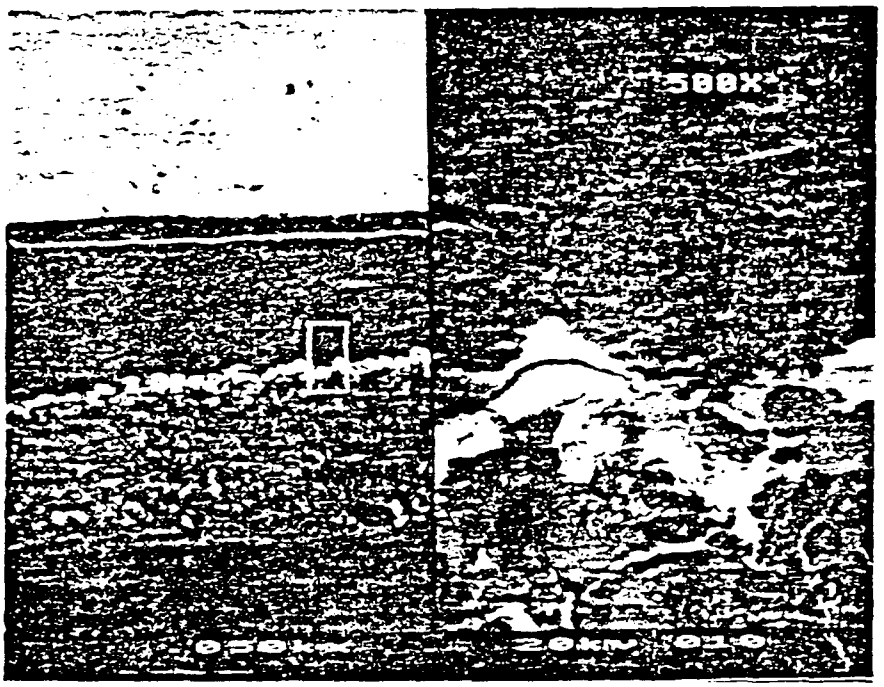


Fig. 1.8b Electron photomicrographs at 50x and 500x of a portion of the cratered surface. The target is viewed here at 0°, and the tungsten carbide layer has a bright appearance.


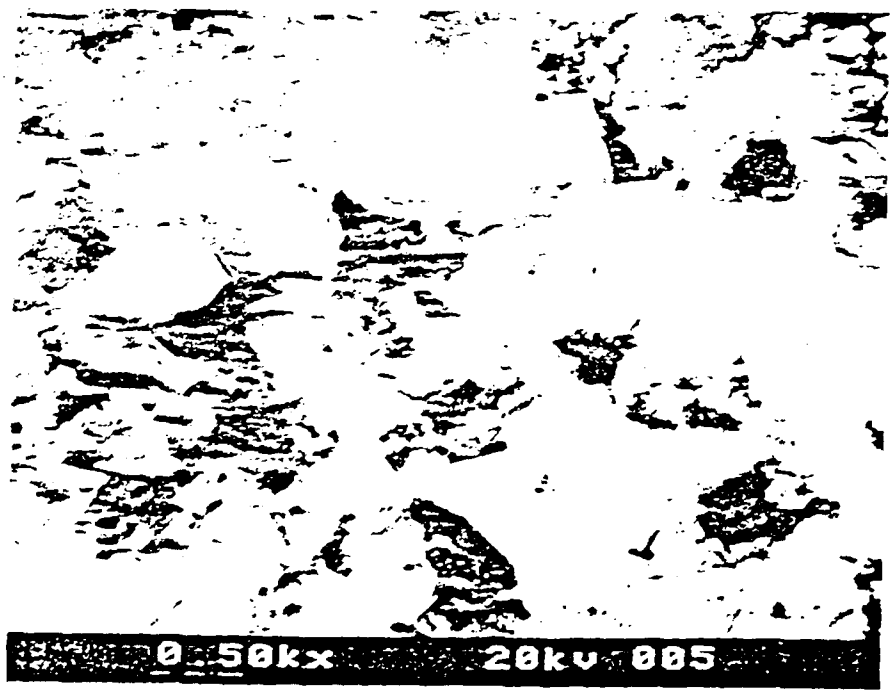


Fig. 2.9 Electron photomicrographs of the target surface in (a) the vaporized region and (b) the unvaporized region.



Fig. 2.10 Cross sections of the coating observed at 500x and 1070x clearly showing the formation of cuplike, hemispherical globules of tungsten carbide.

Since the emissivity measurements suggest that, within the vaporization zone, the tungsten carbide formed a continuous layer, the mechanism by which the underlying carbon was removed is not obvious. Although there appears to be no obstacle to carbon diffusing through the carbide or being transported by a regenerative chemical reaction, such a process would be expected to result in a broad transition or diffusion zone between the regions of pure carbon and pure WC. However, Auger analysis of Fig. 2.10b shows that the transition zone, if it exists, is no thicker than 1 μm, indicating that diffusion is not a likely mechanism. Other possible carbon removal mechanisms are by transport of vapor bubbles, or transport by surface tension driven convection cells. As discussed later, the present data are inadequate to conclusively determine the vaporization mechanism.

# 3. THEORETICAL FLUID MECHANICS STUDIES OF THIN IRRADIATED LIQUID FILMS

## 3.1 Introduction

The protective concept for use as a countermeasure against damage by lasers to satellite systems involves a thin film on top of an ablative substrate. The film is designed to be highly reflective as well as transmissive to the substrate vaporization products. It must remain intact throughout an engagement event and, because the film will be liquid at the elevated temperatures of interest, it must behave as a "liquid surface catalyst."

Two major hydrodynamic questions need to be addressed for this liquid film. The first question is: "What are the physical conditions that provide a stable film behavior?" And secondly, "How is the significant substrate mass transferred across the stable film? Both of these issues have been examined theoretically and the results of the study are described in detail.

The post-test analysis of the e-beam feasibility experiments revealed that the film remains intact and that the film accommodates the substrate mass transfer. In the experimental section of this report the observations relating to film integrity were described. The post-irradiated surface was shiny (metallic-like) and a surface pattern (or structure) was visually observed. A magnified view of the solidified surface appeared to indicate a scalloped surface with somewhat regularly spaced depressions and upwellings; such characteristics are remindful of the tessallations observed on top of a liquid surface undergoing convective motion (see Fig. 3.2). The e-beam experiments also revealed a significant mass loss from the substrate, as shown schematically in Fig. 3.1. Nonuniformity of the e-beam energy deposition is responsible for the non-uniformly ablated surface cross section.

## 3.2 Summary of Fluid Mechanics Studies

Several potential physical mechanisms have been developed to account for the experimental observations. A key finding of our theoretical effort is

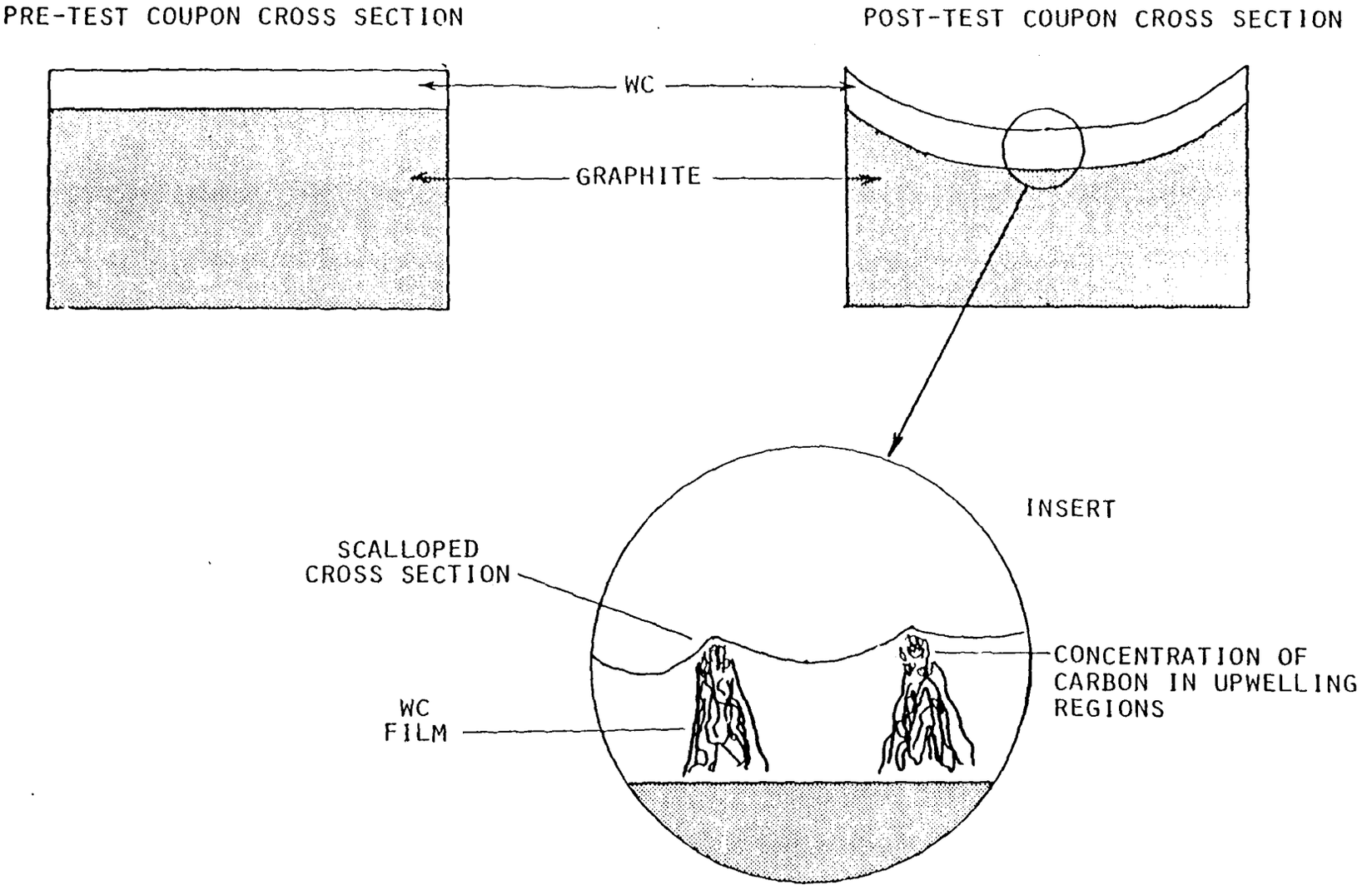


Fig. 3.1 Schematic of surface after e-beam test.

that surface-tension gradient convection cells are driven in the liquid film under the conditions of our experiments. Furthermore, it is likely that intermittent substrate exposure (via bubble breaking or "boiling", for example) occurred in order to provide the substantial mass loss of the substrate. The film stability matters are discussed in Section 3.3 whereas the mass transfer mechanisms are considered in Section 3.4.

## 3.3 Film Stability

### Definition of Stability

The concept of flow stability (or instability) can have various interpretations depending upon the exact nature of the problem. For the thin liquid film concept, the following working definition will be used: A protective liquid film covering a substrate will be considered stable if the film remains intact, without exposing the substrate for any significant period of time. The time qualification allows for the possibility of "boiling" the substrate vapor directly away during bubble-breakup events. This definition implies that a film which is entirely removed either slowly or rapidly is considered unstable. The question of film stability as defined above naturally divides into the cases of no flow and flow (or liquid motion) in the film.

### Stability Under NO Flow Conditions

In the case of no flow, the potential for catastrophic film instability is large, since the gas produced by the vaporization of the substrate can accumulate and generate a pressure which blows the film away from the substrate. Such an accumulation process would occur if the rate of carbon vapor generation were faster than the transport rate of carbon through the film. Diffusion is an unlikely transport mechanism due to the rather small diffusion coefficients D for liquid metals, i.e., $O(10^{-5}\ cm^2/s)$. It would require about 10 s to diffuse an initial carbon molecule across the film thickness d, (= 0.01 cm) since $t_{diff} \sim d^2/D$. The e-beam experiments revealed that 0.02 g of carbon are transferred (lost) with a few seconds of e-beam irradiation at about 4 $kW/cm^2$. Another mechanism must be responsible for the large mass transfer through the film.

In the no flow case, a membrane stability condition for the film may be written. In order for substrate pressure, i.e., gas pressure underneath the liquid film to blow the film off, the force exerted on the film must exceed the surface tension that keeps the liquid adhering to substrate plus the weight of the film (if the film is horizonal). Hence, the blow-off condition is

$$P_{sub}A_f > \rho V_f g_o + \pi D_f \sigma \tag{3.1}$$

where $P_{sub}$ is the substrate pressure, $A_f$, $V_f$, $D_f$ are the area, volume, and diameter of the film, $\rho$ is the film density and $\sigma$ is the surface tension. Equation (3.1) can be rewritten as

$$P_{sub} > \rho d g_o + 4 \frac{\sigma}{D_f} \tag{3.2}$$

where d is the film thickness. The r.h.s. is dominated by the surface tension term, $4\ \sigma/D_f$. The value of $P_{sub}$ for film removal is estimated to be $2 \times 10^{-3}$ atm. The vapor pressure for graphite ($C_3$) vaporization at 3300 K is about $4.2 \times 10^{-3}$ atm, which is the same order as the restraining pressure. Note that the surface tension $\sigma$ for WC at 3300 K is estimated to be about 500 dynes/cm, a value typical of liquid metals. Consequently, one can only conclude that the film is marginally stable under no flow conditions. The thinnest coating tested (1 mil = 25 μm) did not survive the e-beam irradiation. It is believed that this film blew off becuase no flow was induced within the film. The stability criterion developed below appears consistent with this finding.

The other way that the film could disappear under no flow conditions is by direct vaporization. However, for tungsten or WC this is unlikely due to the low vaporization rate for these metals. Note that the cobalt in the film did disappear due to its higher evaporation rate (about five orders of magnitude larger than W!).

Convection Cell Motion

The preceding comments pertain to the case of no flow, or more precisely, to situations without "induced" flow in the thin film. Motion in the liquid film can be induced by two general mechanisms: convection-cell motions and gas-bubble generated motions. These two categories encompass the mass transfer modes discussed in subsequent paragraphs.

Convection-cell motions are the result of an instability driven by the temperature difference across a thin liquid layer. Below some threshold conditions, a differentially heated liquid experiences no motion. However, once a critical condition (to be defined) exists, motion begins and persists in a regular pattern of film-sized cells (see Fig. 3.2). The driving force can be either buoyancy or surface-tension gradients. In either case the driving force overwhelms the viscous resistance to motion and produces flow. For our experiments, buoyancy is not important as shown below. Note that even though the convection cells are unstable in the classic hydrodynamic sense, they are not unstable in the context of the persistance of the film as defined earlier.

Surface-tension Gradient Driven Convection

The convection cells appropriate for the e-beam experiments are driven by surface-tension gradients or the "Marangoni Effect." Consequently, they form when the Marangoni Number M reaches a critical value. M is defined as

$$M = \frac{\partial \sigma}{\partial T} d^2 \left(\frac{dT}{dn}\right) \frac{1}{\rho \nu \kappa} \qquad (3.3)$$

where $\partial\sigma/\partial T$ is the variation of surface tension with temperature, d is the film thickness, dT/dn is the temperature gradient across the layer ($\Delta T/d$), $\rho$ is the density, $\nu$ is the kinematic viscosity, and $\kappa$ is the thermal diffusivity. The first decisive theoretical effort on this stability problem was undertaken by Pearson[3] in 1958. He computed a critical Marangoni Number $M_c = 80$ for heating from below. This identifies a critical depth for convection cells to appear in the e-beam experiments, i.e.,

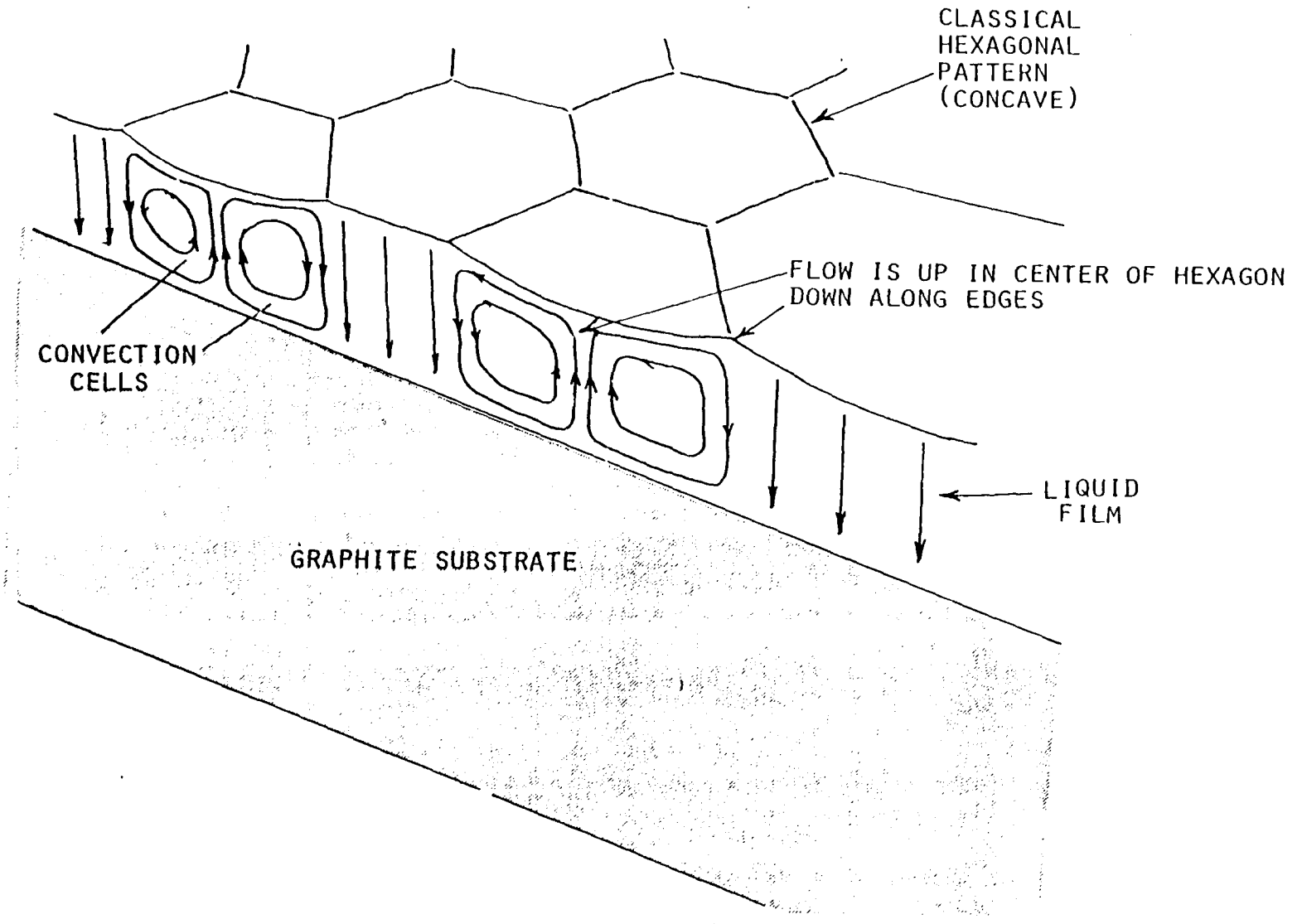


Fig. 3.2 Simultaneous view of film cross section and free surface showing convection cells and classical hexagonal pattern (adapted from Velarde and Normand.[4]

$$d_c^2 = \frac{80\rho\nu\kappa}{\left(\frac{\partial\sigma}{\partial T}\right)\left(\frac{dT}{dn}\right)} \tag{3.4}$$

Only dT/dn is an experimentally determined parameter; the other parameters: $\rho$, $\nu$, $\kappa$ and $\partial\sigma/\partial T$ are intrinsic properties of the liquid film.

It is useful to digress slightly and indicate how the surface tension gradient enters into the hydrodynamic stability problem. The tangential stress balance at an interface between two media leads to the following relation when a gas bounds a liquid

$$\mu\frac{\partial u}{\partial n} = \frac{\partial\sigma}{\partial s} \tag{3.5}$$

where $\mu$ is the viscosity of the liquid, $\sigma$ is the surface tension, u is the liquid film velocity along the surface, n is in the direction normal to the surface and s is along the surface. Since the surface tension depends upon temperature, $\sigma = \sigma(T)$, Eq. (3.5) can be rewritten as

$$\mu\frac{\partial u}{\partial n} = \left(\frac{\partial\sigma}{\partial T}\right)\frac{\partial T}{\partial s} \ . \tag{3.6}$$

A typical value for the surface tension gradient of liquids is -0.2 dyne/cm K. The value is approximately constant. Equation (3.6) states that temperature gradients $\partial T/\partial s$ whether initially present in a flow configuration or induced by convective motions produce a surface flow.

The Marangoni cells develop for liquid layers heated from below (classical Bernard convection) and heated from above (see Ref. 4). Our simulated laser heating is from above. Since gravity (and its direction) is unimportant in the current thin film investigation, the change in sign of the temperature gradient will not alter the physical behavior of these cells in any significant way. A change in sign of the temperature gradient implies a change in sing of the critical Marangoni number with the result that Eq. (3.4) is unaltered.

The critical relationship[4] is shown graphically in Fig. 3.3 as a solid line using estimated values of the physical properties. The behavior of liquid WC or even liquid W is not well-known at the high temperatures of interest ($\approx$ 3300 K). For this reason, we have used in Eq. (3.4) the following parameter values which are typical of liquid metals.

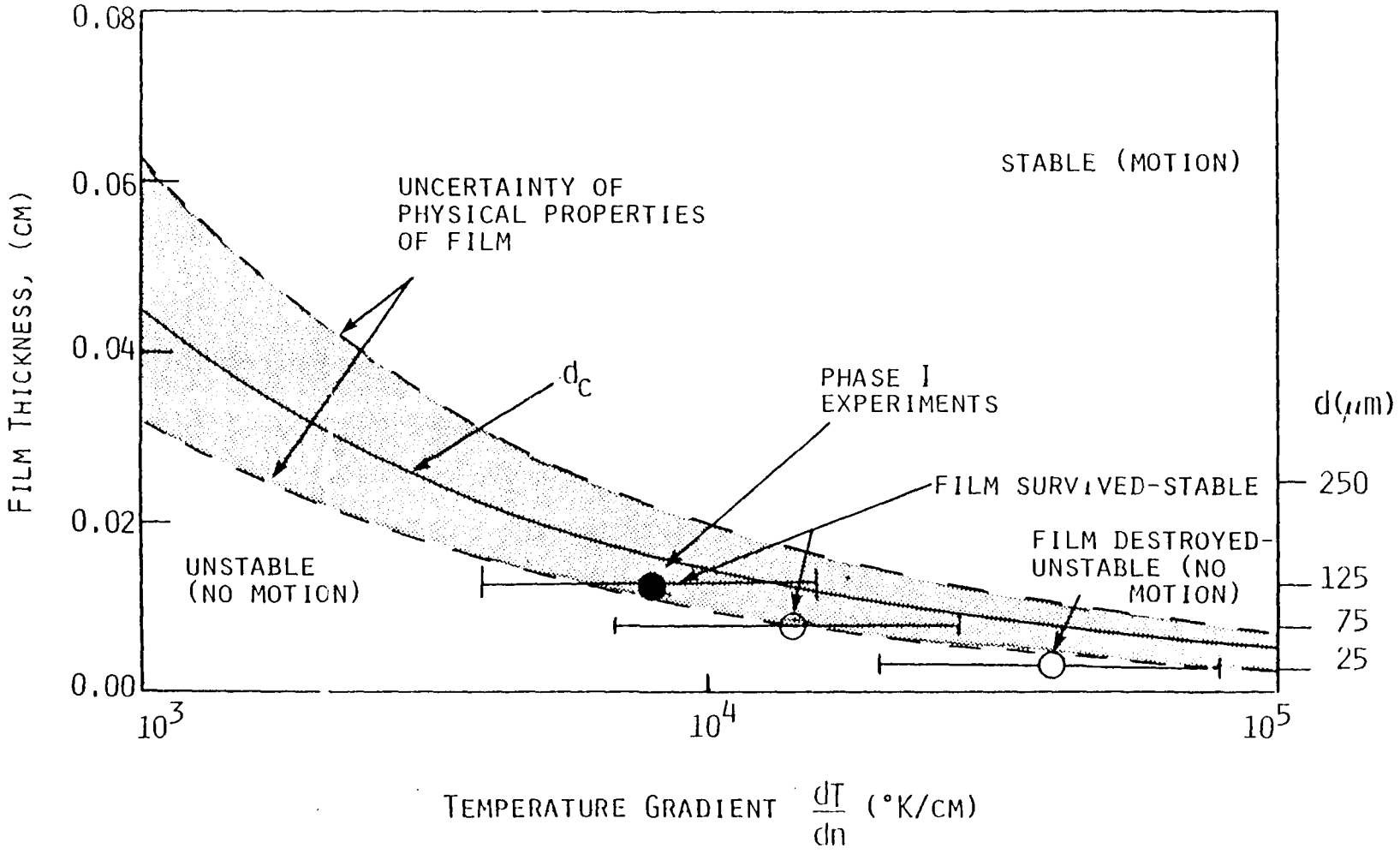


Fig. 3.3 Critical film thickness for surface-tension driven cells.

$$\rho = 15.6 \text{ g/cm}^3$$

$$\nu = 1.3 \times 10^{-3} \text{ cm}^2/\text{s}$$

$$\kappa = 0.25 \text{ cm}^2/\text{s}$$

$$\frac{\partial \sigma}{\partial T} = -0.2 \text{ dyne/cm K} .$$

These values (excluding the density) are only estimates and hence factor of two uncertainty bands have been shown shaded in Fig. 3.3. For values below $d_c$ there is no motion; for values exceeding $d_c$, instability sets in and convection cells commence. Parameters appropriate to three of the e-beam experiments are also shown with the associated error bars. Since the experimental points fall near the critical boundary, there is reason to believe that the WC film experienced convective cell motion. Indeed, the two solid data points refer to cases where the film remained in tact and suggested convection motion. The open symbol referred to the thinnest coating which did not remain intact and which probably blew off due to lack of motion. Two other facts should be mentioned. The Pearson calculations[3] suggested that the periodic cell structure had a wavelength (or repeat cycle) of 2d and more recent studies[4] have shown that the surface-tension driven instability generates a tessellated surface (see Fig. 3.2) once convection commences. Both of these features appear consistent with the PSI experiments as described earlier.

The critical film thickness presented in Fig. 3.3 can be used as part of a map isolating different regions of behavior. It is more convenient to work with the temperature difference across the liquid film $\Delta T$ rather than the gradient $\Delta T/d$. Consequently, the surface-tension-driven criteria leads to a linear relationship between $d_c$ and $(\Delta T)^{-1}$.

Buoyancy-driven Convection

The criteria for buoyancy-driven convection is provided by achieving a critical Rayleigh number

$$R_c = \frac{\gamma g_o \Delta T d_c^3}{\nu \kappa} \qquad (3.7)$$

where $\gamma$ is the coefficient of thermal expansion of the liquid ($\approx 1 \times 10^{-4}$ K$^{-1}$). $B_c$ has been calculated to be 571 (see Pearson[3]). Hence, the variation of $d_c$ with $\Delta T$ (Eq. (3.7)) can be added to the map. The relation between the two convection criteria reaffirms our previous statement that buoyancy is not important for the liquid films under study.

The lack of importance of buoyancy for our thin film concept is demonstrated below. If one examines the hydrodynamic equations in a liquid layer with a temperature difference that is in the same direction as the gravity vector, then a Boussinesq body force term appears in the gravity-direction momentum equation. If one compares this term to the viscous or pressure gradient terms, one finds that

$$\frac{\text{Buoyancy Force}}{\text{Viscous Force}} \propto B_o \gamma \Delta T \tag{3.8}$$

where $B_o$ is the Bond No. $\left(\equiv \rho g_o d^2 / \frac{\partial \sigma}{\partial T} \cdot \Delta T\right)$. For the 125 μm coating $B_o \gamma \Delta T \approx 1.2 \times 10^{-3}$. Hence, the gravitational (or buoyancy) term is not expected to be important for the films of interest. Furthermore, in space where $g_o$ is very small, buoyancy will be negligible even for relatively thick films.

Film Stability Map

The film stability map (Fig. 3.4) includes the two convection cell boundaries as well as a direct vaporization boundary and a "flow-off" boundary. The vaporization boundary was described previously. There is also a "flow-off" boundary that can be caused by the surface-tension gradient driving the film (flow) sufficiently hard that the substrate becomes exposed.[5]

These various considerations suggest that the preferred operating regime for the liquid film mediated laser interaction concept is in the shaded region between the four boundaries in the convection cell regime. In this region there is, at least, a potential for convective mass transfer. However, it is to be noted that successful operation with the thinnest film possible is desirable. Hence, the region near the lower boundary (as shown) is most interesting.

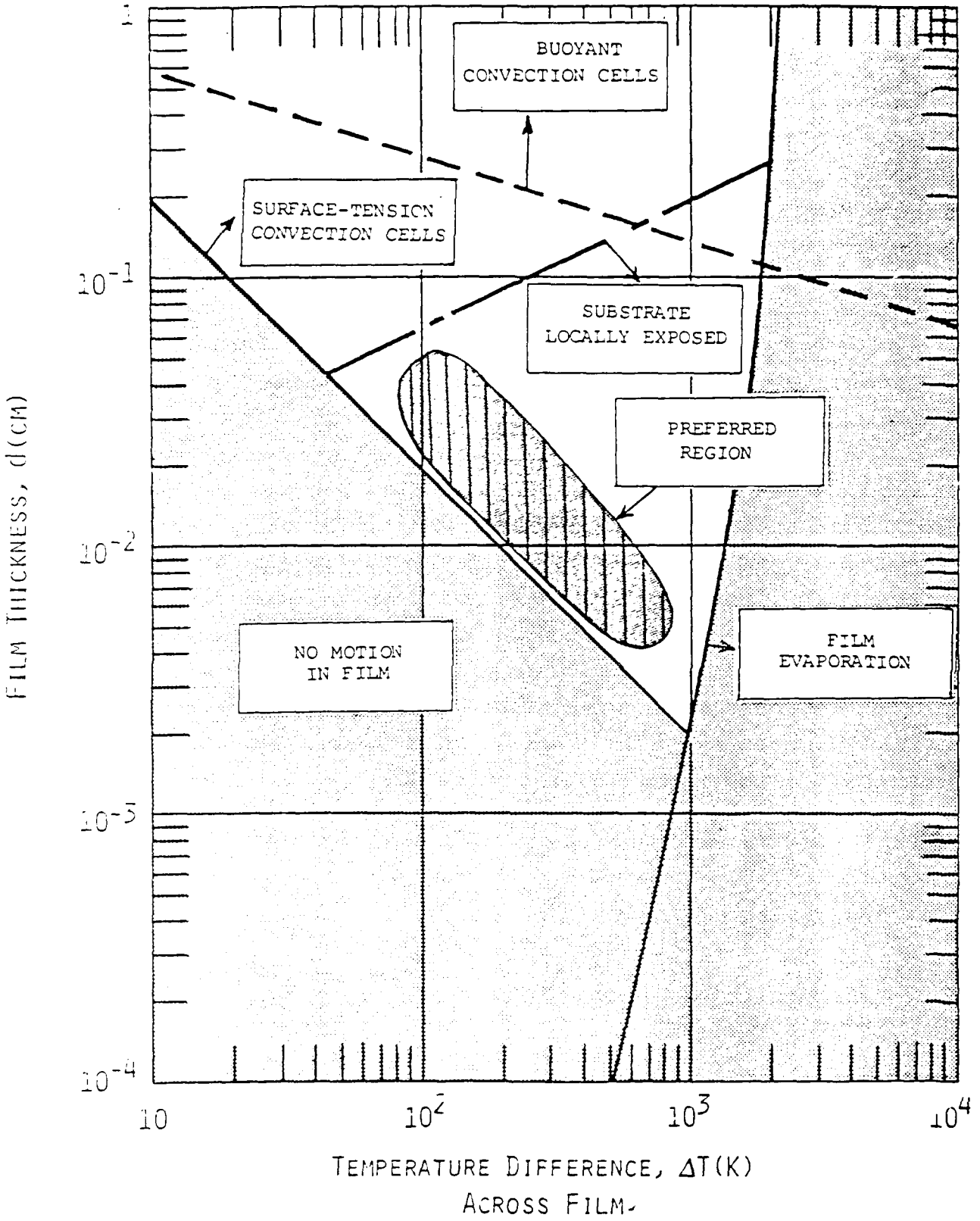


Fig. 3.4 Stable operating regime map.

## 3.4 Substrate Material Mass Transfer

The experiments showed that a substantial amount of substrate graphite was lost from the sample even though the protective WC film remained intact. Organized motion in the film is an obvious requirement for vapor transport since diffusion alone is too slow. Convective motions were described above in relation to film stability; they also play a potentially significant role in the mass transfer issue. The other means for inducing motion is, as mentioned previously, by (carbon) gas-generated bubbles.

There are several ways that bubbles could play a role in the mass transfer process. Two are identified here. Small bubbles could be torn away from the substrate nucleation sites and be convected within the cells toward the surface of the film where the gas would escape. If, however, the surface-tension driven velocities are insufficient to rip the bubbles away from the nucleation sites, then the gas bubbles could continue to grow until they pierced the film surface. In such a case, large mass transfer can occur due to the exposure of the substrate when the bubbles burst. Such behavior would be intermittent since the liquid would rapidly recoat the substrate upon bubble collapse. However, it would be a means to transfer large amounts of gas without destroying the film integrity. This "boiling" mechanism is a very dynamic situation that merits further investigation.

The first matter to explore is the bubble size question. If the bubbles are torn away by the shear provided by the cell motion, then the bubble size at incipient breakaway is[6]

$$a = \frac{8\sigma\varepsilon d}{C_D \rho U^2}^{1/2} \tag{3.9}$$

where $\sigma$ is the surface tension, d is the film thickness, $\varepsilon d$ measures the inhomogeneity (nucleation site) dimensions of the substrate ($\varepsilon << 1$), $C_D$ is the drag coefficient of the bubble, $\rho$ is the liquid density and U is the cell velocity. Equation (6) results from the balance of the surface tension force and the drag force on the bubble. For the Reynolds number range of interest,

O(100), $C_D \approx 0.5$. It is then possible to compute $a$ using the physical properties of the film and the cell velocity. The characteristic velocity, $U \approx 12.7$ cm/s is calculated using the surface-tension boundary condition. Hence, $a(cm) = 1.78\ [\varepsilon d(cm)]^{1/2}$ and the ratio of the bubble size to the film thickness as a function of $\varepsilon$ is given below for the 125 μm film, i.e.,

| $\varepsilon$ | $a/d$ |
|---|---|
| $10^{-2}$ | 1.6 |
| $4 \times 10^{-3}$ | 1.0 |
| $10^{-3}$ | 0.5 |
| $10^{-4}$ | 0.16 |
| $10^{-5}$ | 0.05 |

These results imply that the surface roughness can play a large role in the bubble sizes that are liberated. A 1% inhomogeneity scale ($\varepsilon = 10^{-2}$) is about as large as can be expected; this value leads to a large bubble size (1.6 times larger than the film thickness). Small bubbles 1/20 of the film thickness are obtained for very smooth surfaces ($\varepsilon = 10^{-5}$). If a spectrum of $\varepsilon$ exists, a variation of bubble sizes will also be present.

A natural question that arises is how well would bubbles transfer gas through the film. The mass of a single bubble with diameter equal to the film thickness is about $1.9 \times 10^{-13}$ g. Thus, from the observed mass loss rate (0.002 g/s), 0.02 g were lost during a 10 s run. Hence, $1.04 \times 10^{11}$ such bubbles would have to be liberated in order to account for the mass transfer. At any particular instant, about 3700 bubbles would cover the surface area (0.78 $cm^2$). The matter that remains is how often would one be able to repeat the generation process. For a bubble velocity of 100 cm/s, about $7.9 \times 10^4$ cycles of bubble generation would be possible. Hence, only $2.8 \times 10^{-3}$ of the required bubbles (or mass) could be transfered in this fashion. In other words, an additional mechanism is needed. A possible way to accommodate extra mass loss is to expose the substrate after the bubble has burst. This could permit a "burst" of direct mass loss (substrate vaporization) followed by a subsequent bubble growth and collapse sequence. Further quantitative investigations of the "boiling" regime are certainly warranted.

Based upon the film stability and the bubble calculations, three potential mechanisms for mass transfer have been identified. The flow fields appropriate for these three mechanisms are illustrated in Fig. 3.5.

Convection Cells

In this flowfield configuration, the presence of convection cells is postulated based upon our hydrodynamic stability studies. A regenerative corrosion reaction would occur within the liquid film. This mechanism takes solid carbon, reacts it with the film liquid, transports the carbon to the free surface where carbon gas is liberated. This mechanism is the least likely of the three to explain the high mass loss.

Two-Phase Convection Cells

Earlier, it was shown that under some conditions relatively small bubbles (1/20 film thickness) would be torn from the substrate nucleation sites. This suggests that small bubbles could be transported from the substrate surface to the free surface by the action of convection cells. Since the bubbles are so small, one can permit them to follow the same cell-flow streamlines identified in the convection cell model. Bubble dynamics are important in most cases, however, for small volume fractions of gas within the film, uncoupled computations would be suitable, but, as the volume fraction becomes large, a complex coupled cell-bubble interaction would occur. The next paragraph describes a different mechanism for the critical problem of mass transfer.

Bubbling-Jet Mass Transfer

Perhaps the most important flowfield to consider is one involving bubbles that break when they reach the film free surface and briefly expose the substrate to direct substrate ablation by gas jetting. This flowfield is very complex. It is unsteady and involves several nonlinear, two-phase phenomena that are exceedingly complex. A tractable approach to this problem could be a detailed examination of a single bubble bursting process followed by a jet (gas) flow described by one-dimensional ablation calculations. The amount of time that the direct gas jet is exposed is the key parameter needed to determine the mass transfer for this configuration. Thus, the critical component

5942-5

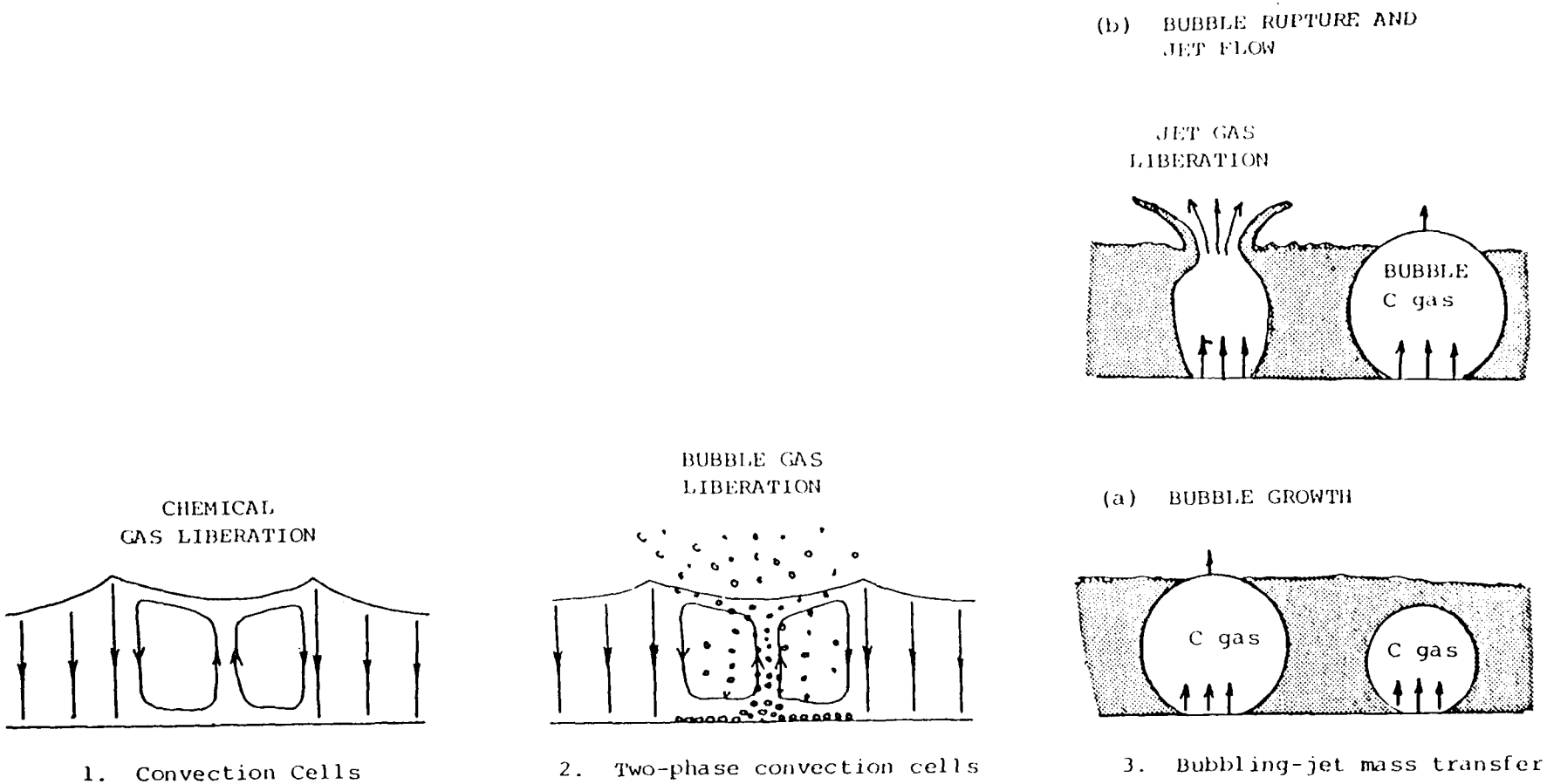


Fig. 3.5 Detailed flowfield configurations.

of the periodic nature of these events is the determination of the time required for the film to reform over the gas ablation region. A statistical analysis could be employed to average such bubble-jet events over the entire surface of the target. The total mass transfer including bubble and jet mass transfer contributions should be comparable with the experimental observations for this mechanism.

Gravitational Effects

The primary application of the thin liquid film concept is to spacecraft which experience a very small gravitational acceleration.[7] This must be contrasted to the experiments on earth. Our experience to date suggests that buoyancy effects are negligible; surface tension dominates.[7,8]

# 4. THERMOCHEMICAL CALCULATIONS

## 4.1 Introduction

Thermodynamic calculations were carried out to determine compositions and vapor pressures of the tungsten-carbon coating. The goal of this effort was to predict equilibrium conditions above the liquid thin film and infer equilibrium vaporization mechanisms. Of particular interest is the form of carbon vaporization, i.e., which carbon vapor species is dominant? Ordinary carbon (graphite) vaporizes as several gaseous species with $C_3$ the dominant species ($C_3 > C_1 > C_2$). This leads to a heat of vaporization of approximately 30 kJ/g. If, however, $C_1$ dominant vaporization occurred (i.e., $C_1 > C_2 > C_3$) the heat of vaporization would be increased to about 60 kJ/gm. Speculations have been made that tungsten carbide coatings might lead to $C_1$ dominant vaporization. This notion is based on predictions for tungsten carbide vaporization. As mentioned earlier, our measurements for heat of vaporization for WC coated graphite indicate $C_3$ dominant (i.e., ordinary graphite) vaporization. Our calculations addressed these issues.

The calculations were done using the SOLGASMIX-PV program from Oak Ridge National Laboratory.[9] The program uses Eriksson's method[10-12] for free energy minimization. The following species were included: (a) solid phase: W, WC, $W_2C$ and C, (b) liquid phase: W, WC, and $W_2C$, and (c) gas phase: $C_1$, $C_2$, $C_3$ and W. The liquid phase components were assumed miscible and treated as ideal solutions. Thermodynamic data for all species except WC and $W_2C$ were obtained from the JANAF tables[13] and their appropriate updates. Data on tungsten carbides are generally not available at higher temperatures (> 3000 K). Thus, lower temperature electrochemically determined free energies[14] were extrapolated. Estimates of free energies of fusion were made from available data on analogous compounds.

The calculations were tested by comparing their results with the proposed phase diagram for the W-C system.[15,16] The calculations succeeded in predicting precipitation of carbon (at high carbon percentages) and precipitation of tungsten (at low carbon content) to within a few percent.

## 4.2 Results

Computed vapor pressures in a W-C system at 3300 K are shown in Fig. 4.1. Vapor pressures for each gaseous species are plotted as a function of atom percentage carbon. Also denoted on the graph are the points at which phase separation occurs (solid carbon precipitation, 47 percent C and solid tungsten precipitation, 88 percent C). The primary points of interest are: (1) at high carbon content when solid carbon is present (as expected) ordinary $C_3$ dominated vaporization occurs, (2) when solid carbon is not present, i.e., vaporization occurs from tungsten carbide, $C_1$ vaporization mostly occurs, and (3) in the tungsten carbide vaporization regime the carbon vapor pressure drops rapidly as the carbon content is decreased.

Since the Phase I experiments indicate heats of vaporization characteristic of $C_3$ vaporization, we may conclude that during vaporization the carbon content was maintained high enough to be very near the carbon precipitation boundary. This may have been achieved by direct transport of carbon vapor from the substrate through the liquid film, i.e., bubbling or a combination of bubbling and tungsten carbide vaporization (for compositions where $C_3$ vaporization occurs). The most significant conclusion of our work is that the transport of carbon vapor through the coating is fast enough that vaporization is determined by the substrate properties and the coating composition seems stable.

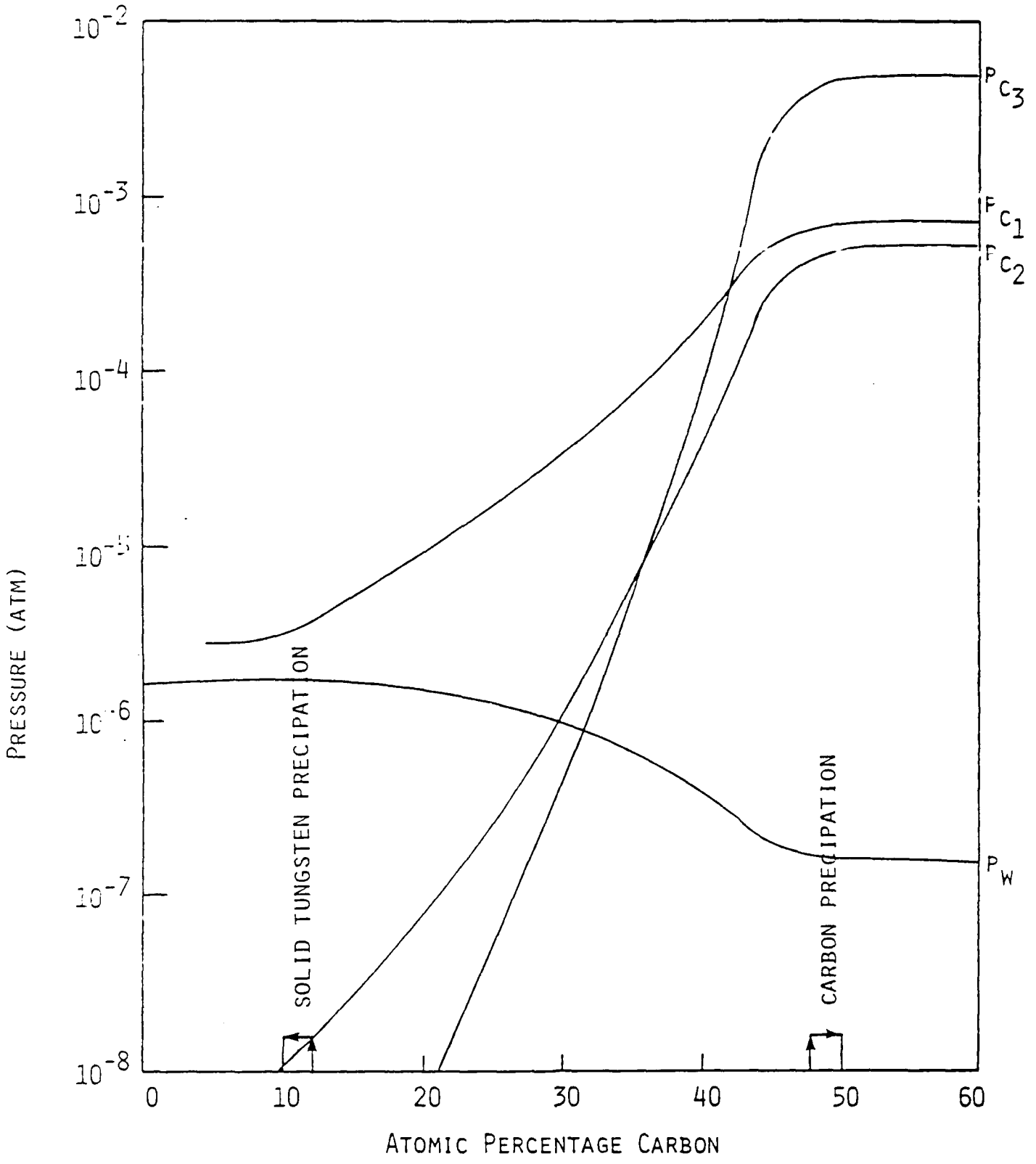


Fig. 4.1 Computed vapor pressures above tungsten carbon mixtures at 3300 K.

## REFERENCES


1. Frish, M. B., "Measurement of High Temperature Thermophysical Properties with Electron-Beam Heating," PSI SR-163, (1983).

2. Frish, M. B. and Nebolsine, P. E., "Metal Bonding with High Intensity Pulsed Lasers," SPIE Proc. 458 (1984). Also, Frish, M. B. and Nebolsine, P. E., "Surface Coating and Alloying by Laser-Induced Heat and Pressure." PSI TR-384 (1983).

3. Pearson, J. R. A., "On Convection Cells Induced by Surface Tension," J. Fluid Mech. 4, Pt. 5, September 1958.

4. Velarde, M. G. and Normand, C., "Convection," Scientific American, July 1980, p. 93.

5. Pimputkar, S. M. and Ostrach, S., "Transient Thermocapillary Flow in Thin Liquid Layers," Phys. Fluids 23, No. 7, July 1980, p. 1281.

6. Silberman, E., "Production of Bubbles by the Disintegration of Gas Jets in Liquid," 5th Midwestern Conference on Fluid Mechanics, U. Michigan, April 1957.

7. Ostrach, S., "Low-Gravity Fluid Flows," Ann. Rev. Fluid Mech. 14, 1982, 313-345.

8. Ostrach, S. and Pradhan, A., "Surface-Tension Induced Convection at Reduced Gravity," AIAA J. 16, No. 5, May 1978.

9. Besmann, T., SOLGASMIX-PV, A Computer Program to Calculate Chemical Systems, ORNL/TM-5775 (April 1977).

10. Eriksson, G., Acta Chem. Scand. 25, 2651(1971).

11. Eriksson, G., Rosen, E., Chemica Scripta, 4, 193(1973).

12. Eriksson, G., Chemica Scripta, 8, 100(1975).

13. JANAF Thermochemical Tables, NBS-NRDS No. 37 (1971) and Supplements.

14. Coltters, R. G. and Belton, G. R., Metal. Trans. A, 14, 1915 (1983).

15. Toth, L. E., Transition Metal Carbides and Nitrides, Academic Press, New York (1971).

16. Storms, E. K., The Refractory Carbides, Academic Press, New York (1967).